doi:10.1016/j.jmb.2009.08.026 J. Mol. Biol. (2009) 393, 113–127

JMB

Available online at www.sciencedirect.com

ScienceDirect

ELSEVIER

The Interaction between Thermodynamic Stability and Buried Free Cysteines in Regulating the Functional Half-Life of Fibroblast Growth Factor-1

Jihun Lee and Michael Blaber*

Department of Biomedical Sciences, College of Medicine, Florida State University, Tallahassee, FL 32306-4300, USA

Received 8 June 2009; received in revised form 11 August 2009; accepted 12 August 2009
Available online 18 August 2009

Protein biopharmaceuticals are an important and growing area of human therapeutics; however, the intrinsic property of proteins to adopt alternative conformations (such as during protein unfolding and aggregation) presents numerous challenges, limiting their effective application as biopharmaceuticals. Using fibroblast growth factor-1 as model system, we describe a cooperative interaction between the intrinsic property of thermostability and the reactivity of buried free-cysteine residues that can substantially modulate protein functional half-life. A mutational strategy that combines elimination of buried free cysteines and secondary mutations that enhance thermostability to achieve a substantial gain in functional half-life is described. Furthermore, the implementation of this design strategy utilizing stabilizing mutations within the core region resulted in a mutant protein that is essentially indistinguishable from wild type as regard protein surface and solvent structure, thus minimizing the immunogenic potential of the mutations. This design strategy should be generally applicable to soluble globular proteins containing buried free-cysteine residues.

Keywords: FGF-1; protein engineering; thermostability; protein half-life; free cysteine

Edited by R. Huber

Introduction

Although accounting for still a comparatively small overall percentage, protein biopharmaceuticals are the fastest-growing category of new drug approvals and currently target over 200 human diseases, including cancers, heart disease, Alzheimer's disease, diabetes, multiple sclerosis, AIDS, and arthritis.[1,2] The impact of protein biopharmaceuticals on US healthcare and the economy is substantial and growing rapidly; however, proteins are a novel type of compound in comparison to traditional small molecules, and they present new and significant challenges to the realization of their full potential as therapeutic agents. One unique property of proteins is that they are capable of adopting different structural conformations, and this profoundly influences critically important properties such as function, solubility, bioavailability, half-life, aggregation, toxicity, and immunogenicity.[3–5] A key intrinsic property of proteins in this regard is thermodynamic stability ($\Delta G_{unfolding}$), which defines the equilibrium between native state and denatured state.

The thermodynamic stability of a protein is of particular significance in therapeutic application because unfolded or aggregated forms of a protein, besides being nonfunctional, are potentially toxic or immunogenic. For example, neutralizing antibodies in patients treated with interferon-α2a were observed when the protein was stored at room temperature and formed detectable aggregates; consequently, both formation of aggregates and immunogenicity were reduced upon storage at 4 °C (where $\Delta G_{unfolding}$ increased[6]). Persistent antibodies were generated in patients treated with human growth hormone with formulations containing 50–70% aggregates; however, when the formulations

*Corresponding author. E-mail address: michael.blaber@med.fsu.edu.

Abbreviations used: FGF, fibroblast growth factor; PEG, polyethylene glycol; PDB, Protein Data Bank; DSC, differential scanning calorimetry; GuHCl, guanidine hydrochloride; DMEM, Dulbecco's modified Eagle's medium; NCS, newborn calf serum; TBS, Tris-buffered saline; ADA, *N*-(2-acetamido)iminodiacetic acid; Tricine, *N*-[2-hydroxy-1,1-bis(hydroxymethyl)ethyl]glycine.

were modified to result in <5% aggregates, only transient or no antibodies were observed.[7] In another study of recombinant clotting factor VIII in mice, the formation of aggregates was associated with the emergence of entirely novel immunogenic epitopes.[8] Thus, protein stability, denaturation, aggregation, and immunogenicity are critical interrelated properties that can determine the successful application of proteins as biopharmaceuticals.

Free-cysteine residues are chemically reactive thiols that are subject to covalent bond formation with other reactive thiols. If present on the solvent-accessible surface of a protein, a free cysteine can potentially participate in a disulfide adduct while the protein maintains its native conformation. However, when present within the solvent-inaccessible core, substantial structural rearrangement must occur to permit accessibility and reactivity. Conversely, the formation of a disulfide adduct involving a buried cysteine is typically structurally incompatible with the native conformation; the resulting misfolded forms can promote aggregation and increased immunogenicity. Due to the negative consequences on protein structure caused by thiol adduct formation of buried free cysteines, mutational substitution of such residues is often accompanied by a notable increase in functional half-life.[9–13]

An analysis of a set of 131 nonhomologous single-domain protein X-ray structures (1.95 Å resolution or better) by Petersen *et al.* reported that the prevalence of free-cysteine residues in proteins is 0.5% (or, typically, one free cysteine in an average size protein); furthermore, 50% of these free cysteines are buried within the protein interior.[14] Thus, although potentially highly problematic for protein therapeutic application, the presence of buried free cysteines in proteins is a surprisingly common occurrence; some familiar examples include fibroblast growth factors (FGFs), interleukin-2, β-interferon, granulocyte colony-stimulating factor, and insulin-like growth factor-binding protein-1 (with the majority of these being approved human therapeutics).

The above narrative highlights two properties of proteins (low thermodynamic stability and buried free-cysteine residues) that can confound successful application of a protein as a biopharmaceutical. In such cases, substantial effort is often exerted to identify appropriate formulations to modulate these intrinsic properties, often with mixed success. A case in point is FGF-1. FGF-1 has poor thermodynamic stability, with a melting temperature (i.e., midpoint of thermal denaturation or T_m) that is marginally above physiological temperature.[15] Because of this intrinsic property, FGF-1 is prone to both aggregation and proteolysis. Furthermore, FGF-1 contains three buried free-cysteine residues that limit functional stability due to reactive thiol chemistry.[11,16,17] However, FGF-1 is a "heparin-binding" growth factor; upon binding heparin, its T_m increases by ~20 °C.[15] Subsequently, it exhibits reduced susceptibility to denaturation-induced aggregation, thiol reactivity, and proteolytic degradation.[15,18] FGF-1 for use as a protein biopharmaceutical (currently in phase II clinical trials for pro-angiogenic therapy in coronary heart disease; NCT00117936) is formulated with the addition of heparin. However, heparin adds considerable expense, has its own pharmacological properties (e.g., it is an anticoagulant), is derived from animal tissues (with associated concerns regarding infectious agents), and causes adverse inflammatory or allergic reactions in a segment of the population. Thus, formulation efforts to modulate the physical properties of a protein are often difficult to achieve and can introduce undesired additional cost or side effects; an alternative approach to formulation is to directly alter the physical properties of a protein by chemical modification or mutagenesis.

Covalent attachment of polyethylene glycol (PEG; a highly soluble, biocompatible polymer) can substantially increase the molecular mass of a protein and thereby reduce renal clearance (i.e., glomerular filtration of biomolecules is size dependent), substantially increasing circulating half-life.[19,20] Furthermore, the attached PEG molecule can physically mask regions of the protein that would otherwise be susceptible to proteolytic attack or immune recognition, further increasing the circulating half-life and reducing immunogenicity.[21,22] PEGylation typically does not increase formal thermodynamic stability and has been noted in some cases to reduce thermodynamic stability;[22,23] thus, the beneficial properties of PEGylation are primarily associated with modulation of renal clearance and reduction of the irreversible pathways associated with degradation and insolubility. One detriment of PEGylation is that it typically interferes with critical functional interfaces on the protein surface, often reducing receptor/ligand affinity by two or more orders of magnitude; however, one of the notable results from PEGylation studies is that shielding epitopes on the protein surface can substantially reduce or eliminate their immunogenic potential. This has important ramifications for protein engineering, suggesting that mutations at solvent-inaccessible positions within proteins may limit their immunogenic potential.

Mutating proteins to improve properties for human therapeutic application is a viable approach: over 30 mutant forms of proteins have been approved by the US Food and Drug Administration for use as human biopharmaceuticals.[24] These include mutations that contribute to increased yields during purification, increased *in vivo* functional half-life, or increased specific activity. Examples include mutations of buried free-cysteine residues in β-interferon (Betaseron®) and interleukin-2 (Proleukin®), as well as others hypothesized to increase thermostability. Thus, a mutational approach to improving the physical properties of proteins is a viable route for developing "second-generation" protein biopharmaceuticals. In this regard, mutations within proteins that eliminate buried free cysteines and increase thermostability are of particular interest, since they can directly influence key physical properties that determine functional half-

life, resistance to proteolytic degradation, solubility and aggregation, and immunogenic potential.

In this report, we study the relationship between protein stability and buried free cysteines in influencing the functional half-life of FGF-1. The results demonstrate a key interactive relationship between thermostability and buried free cysteines in effectively regulating protein functional half-life. Furthermore, we explore a strategy for increasing thermostability by introducing mutations within the solvent-excluded interior of the protein that eliminate or improve upon packing defects within the wild-type structure. The results show that significant stability gains can be realized using this strategy, and that such increases in thermostability can be achieved with minimal perturbation of the overall wild-type protein structure, including surface features and solvent structure. In a study of combined mutations, we show how such stabilizing core packing mutations can be combined with mutations that eliminate buried free cysteines to produce a 40-fold increase in functional half-life while simultaneously maintaining wild-type surface features and solvent structure. Such mutations identify a general protein design strategy whereby functional half-life can be manipulated while minimizing immunogenic potential.

Results

Mutant protein purification

All mutant proteins were expressed and purified to apparent homogeneity and with a yield similar to that of the wild-type protein (20–40 mg/L).

X-ray structure determination

Diffraction-quality crystals were obtained for the Leu44→Trp, Phe85→Trp, Phe132→Trp, Val31→Ile, and Cys117→Ile point mutations; the Leu44→Phe/Phe132→Trp double mutant; and the Leu44→Phe/Cys83→Thr/Cys117→Val/Phe132→Trp quadruple mutant. Each of these mutant proteins crystallized in the wild-type orthorhombic $C222_1$ space group with two molecules in the asymmetric unit and in each case yielded data sets with 1.9–2.0 Å resolution. Crystal structures were refined to acceptable crystallographic residuals and stereochemistry (Table 1). A brief description of each refined structure follows; however, in the presentation of results, a description of packing defects (i.e., cavities) within the core of the wild-type protein is necessary. The wild-type FGF-1 protein

Table 1. Crystallographic data collection and refinement statistics

	Leu44→Trp	Phe85→Trp	Phe132→Trp	Val31→Ile	Cys117→Ile	Leu44→Phe/Phe132→Trp	Leu44→Phe/Cys83→Thr/Cys117→Val/Phe132→Trp
Space group	$C222_1$	$C222_1$	$C222_1$	$C222_1$	$C222_1$	$C222_1$	$C222_1$
Cell constants (Å)	a=73.8, b=97.6, c=108.8	A=74.2, b=95.8, c=109.6	a=74.4, b=96.0, c=108.9	a=73.9, b=97.4, c=108.8	a=74.7, b=97.2, c=108.1	a=73.2, b=97.6, c=108.5	a=74.4, b=96.0, c=108.4
Maximum resolution (Å)	2.0	1.9	1.95	2.0	2.0	1.9	1.95
Mosaicity (°)	0.53	1.00	0.96	0.44	0.50	0.60	0.68
Redundancy	6.5	7.0	5.8	5.6	9.0	12.9	13.2
Molecules per asymmetric unit	2	2	2	2	2	2	2
Matthew coefficient (Å^3/Da)	2.97	2.95	2.95	2.97	2.98	2.94	2.93
Total reflections	169,561	214,161	164,516	146,083	242,167	398,874	368,957
Unique reflections	25,975	30,761	28,568	26,232	26,839	30,802	27,994
I/σ (overall)	42.4	32.2	30.2	32.0	30.4	35.7	56.2
I/σ (highest shell)	7.3	3.6	3.6	3.7	3.3	3.8	8.6
Completion overall (%)	96.2	98.7	99.1	97.2	99.4	99.3	97.3
Completion highest shell (%)	70.7	89.2	99.1	95.6	94.5	91.9	78.6
R_{merge} overall (%)	6.2	7.9	6.2	7.8	9.1	7.3	5.6
R_{merge} highest shell (%)	18.3	37.9	31.0	28.8	38.7	35.0	19.4
Nonhydrogen protein atoms	2284	2278	2278	2254	2276	2284	2288
Solvent molecules/ion	174/17	238/15	235/12	186/10	187/15	199/14	224/14
R_{cryst} (%)	20.7	18.8	19.0	19.9	19.8	19.0	20.6
R_{free} (%)	24.3	22.8	21.3	23.3	23.1	22.1	23.8
RMSD bond length (Å)	0.009	0.009	0.008	0.010	0.009	0.009	0.006
RMSD bond angle (°)	1.4	1.5	1.4	1.5	1.5	1.4	1.3
Ramachandran plot							
Most favored (%)	90.4	92.5	93.4	89.5	89.5	92.5	90.4
Additionally allowed (%)	9.2	7.5	6.6	9.6	10.1	7.0	9.6
Generously allowed (%)	0.4	0.0	0.0	0.9	0.4	0.4	0.0
Disallowed (%)	0.0	0.0	0.0	0.0	0.0	0.0	0.0
PDB code	3FJC	3FJ9	3FJA	3FJB	3FJ8	3FJD	3FGM

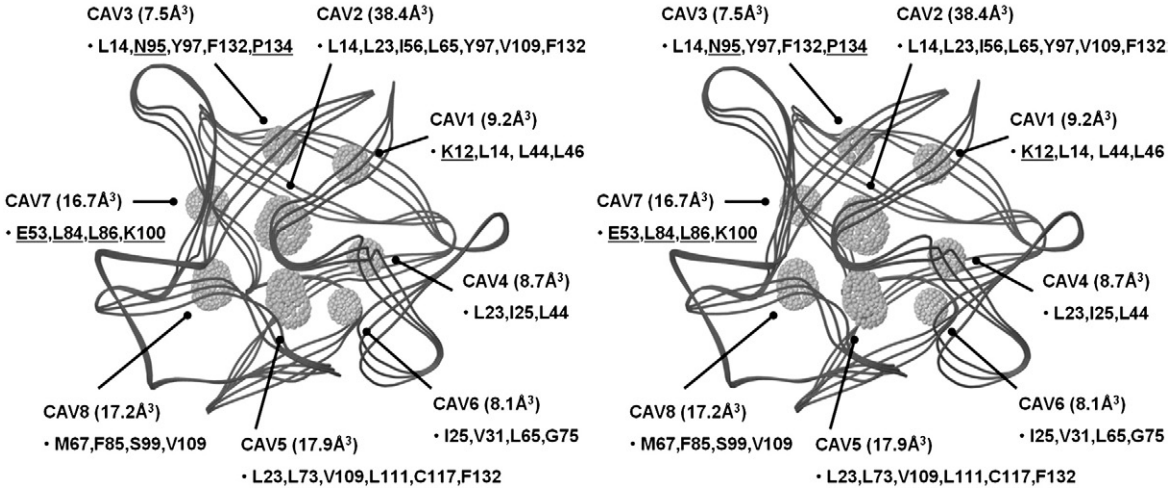

Fig. 1. Relaxed stereo ribbon diagram of wild-type FGF-1 (PDB code 1JQZ; molecule A) indicating the location of the eight solvent-excluded cavities identified using a 1.2-Å-radius probe. Residues bordering the cavities are indicated in single-letter amino acid codes, and underlined residues have solvent accessibility.

[Protein Data Bank (PDB) code 1JQZ; molecule A] contains eight cavities, which are detectable using a 1.2-Å-radius probe. These cavities are identified by number ("cav1" through "cav8"), and details of their volume and location are given in Fig. 1.

Leu44→Trp

The mutant Trp side chain at position 44 is adopted with a $\chi_1 = -56°$ (similar to that of the wild-type Leu44: $\chi_1 = -44°$) and a $\chi_2 = 90°$ (which differs from that of the wild-type Leu44: $\chi_2 = 165°$) (Fig. 2a). Cav4 lies adjacent to the side chain of position 44, and the C^{Z2} atom of the mutant indole ring occupies this region and effectively fills this cavity. The mutant Trp, however, introduces a close contact with the adjacent Ile side chain at position 25, which responds by rotating from a *gauche*+ to a *trans* rotamer. In this orientation, the Ile25 $C^{\delta 1}$ atom occupies the adjacent cav6. This reorientation of the Ile25 side chain to accommodate the mutant Trp also involves a 1.0-Å shift of the Ile25 main-chain C^{α} away from position 44, leading to an apparent increase in the Ile25N-His41O interchain H-bond distance from 3.1 to 3.3 Å. The nitrogen in the indole ring of the mutant Trp H-bonds with the main-chain carbonyl of residue Leu23 and is achieved with minimal structural perturbation.

Phe85→Trp

The mutant Trp side chain at position 85 is adopted with a $\chi_1 = -61°$ (essentially identical with that of the wild-type Phe85: $\chi_1 = -65°$) and a $\chi_2 = 95°$ (identical with that of the wild-type Phe) (Fig. 2b). Cav8 lies adjacent to the side chain of position 85, and the C^{Z3} atom of the mutant indole ring occupies this region and substantially fills this cavity. Accommodation of the mutant Trp is associated with minimal perturbation of the surrounding structure. The nitrogen in the indole ring of the mutant Trp H-bonds with the main-chain carbonyl of residue Leu65 and is achieved with minimal structural perturbation.

Phe132→Trp

The mutant Trp side chain at position 132 is adopted with a $\chi_1 = -59°$ (similar to that of the wild-type Phe132: $\chi_1 = -68°$) and a $\chi_2 = 85°$ (essentially identical with that of the wild-type Phe132: $\chi_2 = 89°$) (Fig. 2c). Two cavities are located adjacent to position 132: cav2 lies beneath the aromatic ring of Phe132 (and is the large central cavity characteristic of the β-trefoil architecture[25]), and cav5 is adjacent to the introduced Trp C^{Z2} atom. The mutant Trp side chain partially fills both these cavities. Accommodation of the mutant indole ring is associated with minimal perturbation of the surrounding structure. There is a slight rotation of the χ_2 angle of adjacent Leu111, as well as slight repositioning of the main-chain carbonyl of adjacent residue Leu14; both of these structural adjustments are in a direction away from the mutant indole ring. The nitrogen of the indole ring in the mutant Trp H-bonds with the main-chain carbonyl of residue Val109 and is achieved with minimal structural perturbation.

Fig. 2. Relaxed stereo diagrams of the Leu44→Trp mutant (a), Phe85→Trp mutant (b), Phe132→Trp mutant (c), Val31→Ile mutant (d), and Cys117→Ile mutant (e) overlaid onto the wild-type FGF-1 (PDB code 1JQZ) structure (dark gray). Also shown are cavities adjacent to these mutant positions within the wild-type structure that are detectable using a 1.2-Å-radius probe (see Fig. 1 for details).

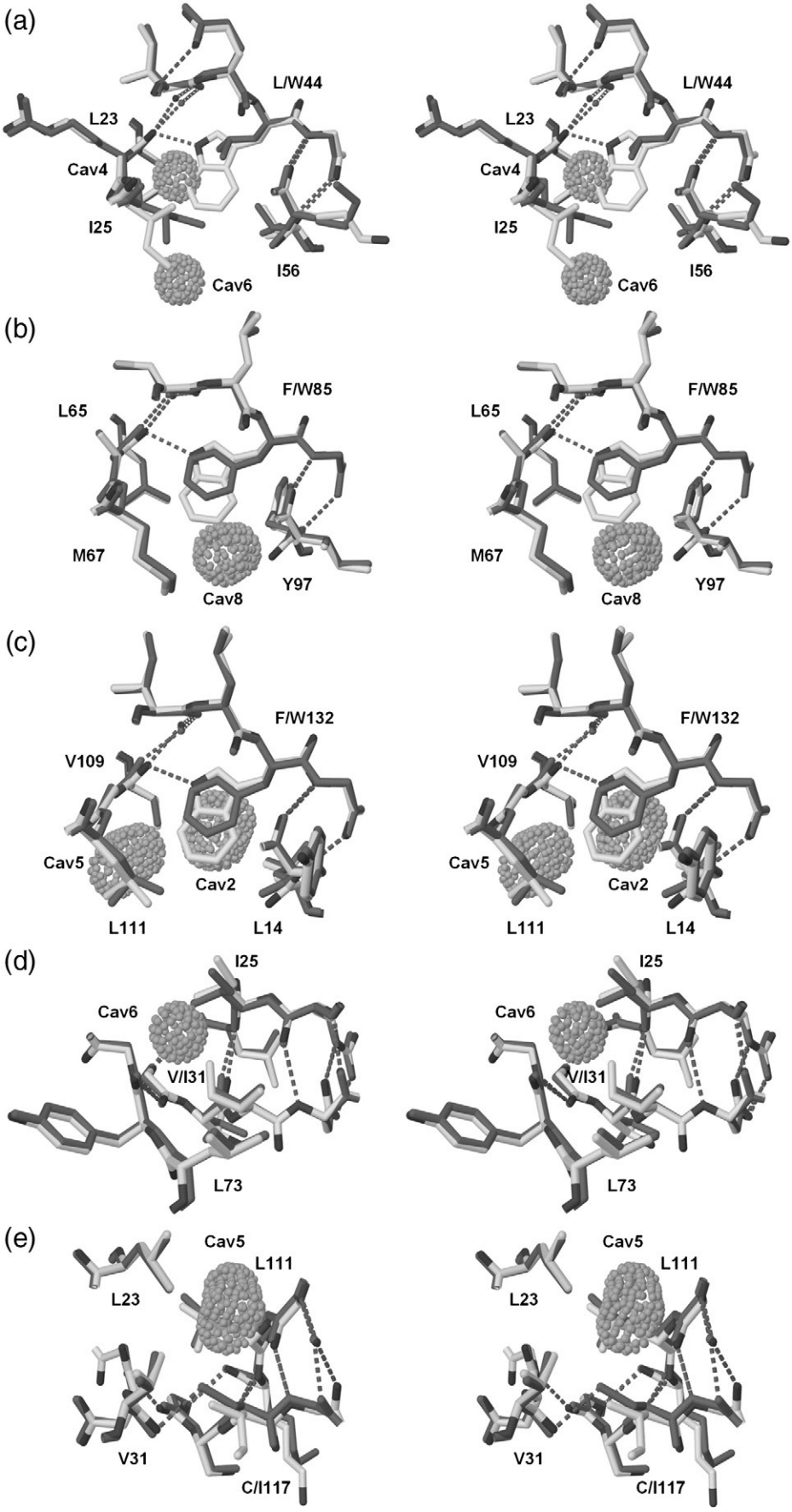

Fig. 2 (*legend on previous page*)

Val31→Ile

The mutant Ile side chain at position 31 adopts a $\chi_1 = -55°$ (essentially overlaying the wild-type Val side chain at this position) and a $\chi_2 = -60°$ (Fig. 2d). Cav6 lies adjacent to the introduced Ile $C^{\delta 1}$ atom, but is only partially filled. However, in response to the introduction of the mutant Ile $C^{\delta 1}$ at position 31, adjacent residue Ile25 shifts in a direction away from position 31 such that the C^{β}–C^{β} distance between these neighboring groups increases from 5.6 to 6.1 Å. Thus, while the mutant Ile side chain partially fills an adjacent cavity, its accommodation is associated with positional adjustment of neighboring side chains.

Cys117→Ile

The mutant Ile side chain at position 117 adopts a $\chi_1 = 49°$ (essentially overlaying the mutant Ile $C^{\gamma 2}$ atom onto the wild-type Cys S^{γ} atom) and a $\chi_2 = -175°$ (Fig. 2e). Cav5 is adjacent to position 117; however, the χ_2 rotamer adopted by the mutant Ile side chain positions its $C^{\gamma 1}$ and $C^{\delta 1}$ atoms away from this cavity. The Ile mutation therefore has no effect on the size of adjacent cav5. Furthermore, this orientation for the mutant Ile side chain positions the $C^{\gamma 1}$ and $C^{\delta 1}$ atoms outside of the core region, and these atoms become solvent accessible.

Leu44→Phe/Phe132→Trp

The structural effects of the Leu44→Phe point mutant have been previously reported.[26] Briefly, the introduced Phe aromatic ring essentially fills cav4, and the adjacent Ile25 side chain retains its rotamer orientation but shifts position away from Phe44 and fills cav6. Positions 44 and 132 are not adjacent packing neighbors, and residues Leu14 and Leu23 are sandwiched between them. The structural effects of the Phe132→Trp point mutant have been described above, and the Leu44→Phe/Phe132→Trp double mutant can be described as comprising the additive effects of constituent point mutations. In this regard, this combined double mutant effectively fills cav4 and cav6 and partially fills cav 2 and cav5 (Fig. 3a).

Leu44→Phe/Cys83→Thr/Cys117→Val/Phe132→Trp

The structural effects of the Cys117→Val point mutant have been previously reported.[27] Structural and thermodynamic details of the Cys83→Thr point mutant are discussed in our accompanying report.[28] However, briefly, the $C^{\gamma 2}$ atom of the mutant Thr83 side chain juxtaposes the wild-type Cys S^{γ} atom and, in this orientation, the H-bond interaction with the main-chain amide of position Asn80 is lost, and this amide appears as an unsatisfied H-bond donor. The Cys83→Thr point

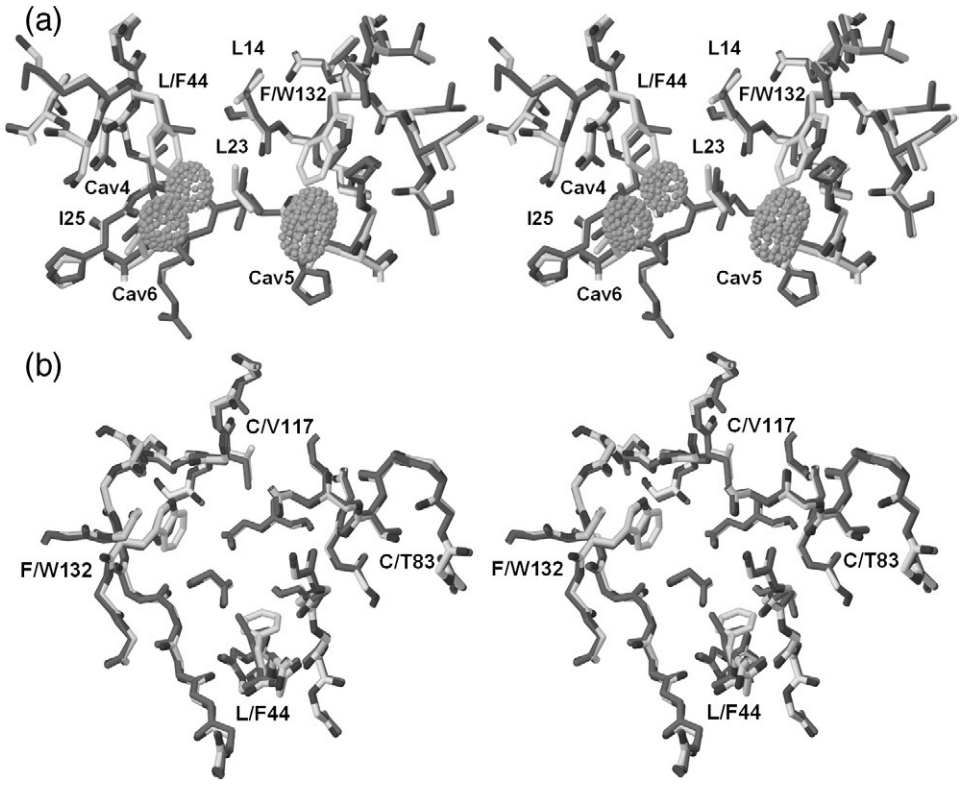

Fig. 3. Relaxed stereo diagrams of the Leu44→Phe/Phe132→Trp double mutant (a) and the Leu44→Phe/Cys83→Thr/Cys117→Val/Phe132→Trp quadruple mutant (b) overlaid onto the wild-type (PDB code 1JQZ) FGF-1 structure (dark gray). (a) also shows the location of the cavities (cav4, cav5, and cav6) that are either filled, or partially filled, in response to the Leu44→Phe/Phe132→Trp double mutation (partially-filled cav2 is omitted for clarity). In (b), the overlay with the wild-type structure shows only the main-chain atoms within 5 Å of positions 44, 83, 117, and 132.

mutant thus destabilizes the protein by 5.2 kJ/mol. The Leu44→Phe/Phe132→Trp double mutant has been described above. None of these four positions within the core region of the protein is an adjacent packing neighbor, and the effects of the combined mutations can be described as comprising the additive effects of the constituent point mutations. The Cys83→Thr and Cys117→Val mutations do not affect any of the eight identified cavities in the structure, and the cavity-filling properties of this quadruple mutant are essentially identical with those observed for the Leu44→Phe/Phe132→Trp double mutant. These four mutations within the core region are accommodated with essentially no detectable change in the overall structural backbone; an overlay of the set of all main-chain atoms within 5 Å of positions 44, 83, 117, and 132 yields an RMSD of 0.23 Å (i.e., essentially the error of the X-ray data set; Fig. 3b).

Isothermal equilibrium denaturation and differential scanning calorimetry

The isothermal equilibrium data for the mutant proteins in each case exhibited excellent agreement with a two-state model. The Trp mutations at positions 44, 85, and 132 exhibit differential effects on protein stability: Leu44→Trp destabilizes the protein by 3.4 kJ/mol, Phe85→Trp is essentially neutral, while Phe132→Trp stabilizes the protein by −1.6 kJ/mol (Table 2). Both the Val31→Ile (4.0 kJ/mol) mutation and the Cys117→Ile mutation (1.5 kJ/mol) destabilized the protein. The combined double mutant of Leu44→Phe/Phe132→Trp stabilized the protein by −3.9 kJ/mol and therefore yielded essentially additive effects on stability in comparison to constituent point mutations.

As previously reported, the Cys117→Val mutation, which effectively removes this buried free cysteine, is only slightly destabilizing (1.2 kJ/mol),[27] while the Cys83→Thr mutation significantly (5.2 kJ/mol) destabilizes the protein.[28] The combined Cys83→Thr/Cys117→Val double mutant, which eliminates two of the three buried free-cysteine residues in the protein, destabilizes by 6.1 kJ/mol (Table 2), essentially an additive effect of the constituent point mutations. Notably, combining the destabilizing Cys83→Thr/Cys117→Val double mutant with the stabilizing Leu44→Phe/Phe132→Trp double mutant yields a quadruple mutant whose stability is indistinguishable from that of the wild-type protein (Table 2); thus, in the Leu44→Phe/Cys83→Thr/Cys117→Val/Phe132→Trp quadruple mutant, two of the three buried free cysteines have been eliminated, while wild-type-equivalent stability has been effectively maintained. The Lys12→Val/Cys83→Thr/Cys117→Val triple mutant combines the destabilizing double-cysteine mutant with a point mutation (Lys12→Val; located in a partially solvent-accessible surface position) that has been shown to stabilize the protein by −7.8 kJ/mol (and fills adjacent cav1).[29] The resulting Lys12→Val/Cys83→Thr/Cys117→Val triple mutant exhibits a stability (−1.9 kJ/mol) that is slightly better than that of wild-type FGF-1 and is essentially the sum of individual point mutations; thus, this combined mutant has also eliminated two of the three buried free-cysteine residues but has improved upon wild-type stability.

Table 2. Thermodynamic parameters for FGF-1 mutants determined from isothermal equilibrium denaturation by GuHCl in ADA buffer

Protein	ΔG (kJ/mol)	*m*-value (kJ/mol M)	C_m (M)	$\Delta\Delta G$[a] (kJ/mol)
Reference proteins				
Wild type[b]	21.1±0.6	18.9±0.6	1.11±0.01	—
Cys117→Val[b]	21.0±0.3	20.1±0.1	1.05±0.01	1.2
Lys12→Val/Cys117→Val[c]	27.7±0.5	18.1±0.3	1.53±0.01	−7.8
Cavity-filling core mutations				
Leu44→Trp	15.1±0.9	16.5±0.7	0.92±0.02	3.4
Phe85→Trp	22.3±0.1	19.7±0.3	1.13±0.01	−0.4
Phe132→Trp	26.1±0.4	22.0±0.5	1.19±0.01	−1.6
Val31→Ile	18.8±0.1	20.7±0.1	0.91±0.00	4.0
Cys117→Ile	20.1±0.5	19.6±0.3	1.03±0.01	1.5
Leu44→Phe[b]	25.1±0.3	20.4±0.2	1.23±0.01	−2.4
Leu44→Phe/Phe132→Trp	24.0±1.0	18.1±0.8	1.32±0.01	−3.9
Buried free-cysteine removal mutations				
Cys83→Thr/Cys117→Val	17.5±0.8	21.7±0.9	0.81±0.01	6.1
Leu44→Phe/Cys83→Thr/Cys117→Val/Phe132→Trp	21.4±0.8	18.9±0.6	1.13±0.01	−0.4
Lys12→Val/Cys83→Thr/Cys117→Val	24.1±0.5	19.9±0.4	1.21±0.01	−1.9

[a] $\Delta\Delta G = (C_{m\ wild\ type} - C_{m\ mutant})(m_{wild\ type} + m_{mutant})/2$, as described by Pace and Scholtz.[44] A negative value of $\Delta\Delta G$ indicates a more stable mutation.
[b] Thermodynamic parameters reported by Brych *et al.*[27]
[c] Thermodynamic parameters reported by Dubey *et al.*[29]

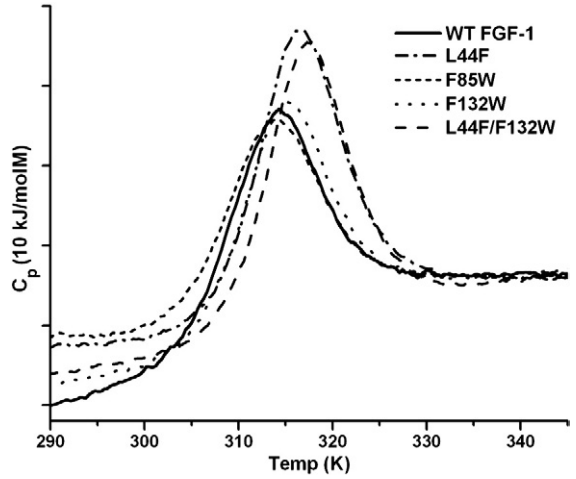

Fig. 4. DSC endotherms for wild-type FGF-1, Leu44→Phe, Phe85→Trp, and Phe132→Trp point mutants, and for Leu44→Phe/Phe132→Trp double mutant. Conditions of analysis are provided in Materials and Methods.

Differential scanning calorimetry (DSC) data were collected for the Leu44→Phe, Phe85→Trp, and Phe132→Trp point mutations, as well as for the Leu44→Phe/Phe132→Trp double mutant (Fig. 4). As reported previously for the wild-type protein, the thermal denaturation was highly reversible (i.e., >80% in each case) and two state (i.e., $\Delta H_{cal}/\Delta H_{vH} \sim 1.0$) when 0.7 M guanidine HCl (GuHCl) was included in the buffer.[30] The $\Delta\Delta G$ values derived from DSC measurements (Table 3) are in excellent agreement with isothermal equilibrium denaturation data (Table 2). The results show that both ΔH and ΔS increase for stabilizing mutations, and both decrease for Phe85→Trp. The $\Delta\Delta G$ values for these mutations positively correlate with $\Delta\Delta H$ and negatively correlate with $-T^*\Delta\Delta S$ in each case; thus, the observed changes in stability for these mutations reflect an enthalpy-driven process. The DSC data are consistent with the introduction of favorable van der Waals interactions for the Leu44→Phe and Phe132→Trp mutants, but not for the Phe85→Trp mutant. The DSC data also confirm the isothermal equilibrium data by showing that the effects on the melting temperature and ΔG of the Leu44→Phe/Phe132→Trp double mutant are essentially additive with respect to constitutive point mutations.

Table 3. DSC data in ADA buffer in the presence of 0.7 M GuHCl

Protein	ΔH (kJ/mol)	ΔS (kJ/mol K)	T_m (K)	ΔT_m (K)	$\Delta\Delta G$ (kJ/mol)
Wild type	275±2	0.88	312.9±0.1	—	—
Leu44→Phe	327±2	1.03	316.0±0.1	3.1	−3.0
Phe85→Trp	266±4	0.85	312.6±0.4	−0.3	0.3
Phe132→Trp	289±2	0.92	314.1±0.1	1.3	−1.2
Leu44→Phe/Phe132→Trp	330±4	1.04	317.0±0.1	4.2	−4.1

Mitogenic activity and functional half-life in unconditioned medium

The mitogenic response of NIH 3T3 cells to wild-type, Cys117→Val, Cys83→Thr/Cys117→Val, Leu44→Phe/Cys83→Thr/Cys117→Val/Phe132→Trp, and Lys12→Val/Cys83→Thr/Cys117→Val mutant proteins, in the presence and in the absence of heparin sulfate, is shown in Fig. 5. Both the wild-type protein and the Cys117→Val mutant protein exhibit a marked decrease in mitogenic activity in the absence of (10 U/ml) exogenously added heparin (Table 4); however, the Cys83→Thr/Cys117→Val, Leu44→Phe/Cys83→Thr/Cys117→Val/Phe132→Trp, and Lys12→Val/Cys83→Thr/Cys117→Val mutant proteins exhibit substantial mitogenic potency even in the absence of exogenously added heparin.

The mitogenic half-life of wild-type, Cys117→Val, Cys83→Thr/Cys117→Val, Leu44→Phe/Cys83→Thr/Cys117→Val/Phe132→Trp, and Lys12→Val/Cys83→Thr/Cys117→Val mutant FGF-1 proteins in response to preincubation in unconditioned Dulbecco's modified Eagle's medium (DMEM)/0.5% newborn calf serum (NCS) is shown in Fig. 6. The wild-type protein displays a

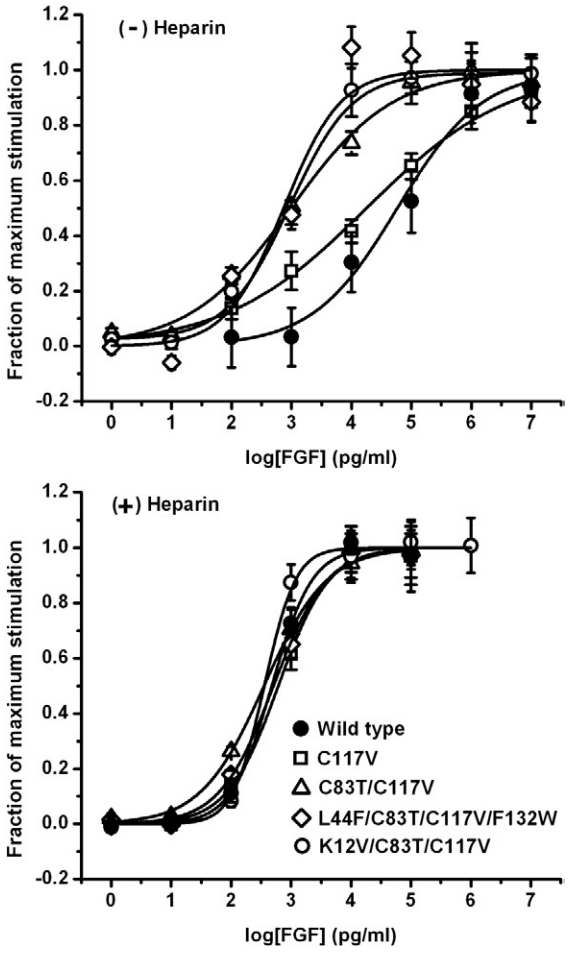

Fig. 5. 3T3 fibroblast mitogenic assay of wild-type and mutant forms of FGF-1 in the absence (top) and in the presence (bottom) of 10 U/ml heparin.

Table 4. Mitogenic activity of mutant forms of FGF-1 in the absence and in the presence of 10 U/ml heparin against NIH 3T3 fibroblasts, protein functional half-life in unconditioned DMEM/0.5% NCS medium, and protein half-life with 200:1 trypsin digestion

	EC_{50} (ng/ml)		Unconditioned medium	200:1 trypsin digestion
Protein	(−) Heparin	(+) Heparin	Half-life (h)	Half-life (min)
Wild type	58.4±25.4	0.48±0.08	1.0	9.8
Cys117→Val	18.0±12.9	0.61±0.12	9.4	9.1
Cys83→Thr/Cys117→Val	0.98±0.78	0.35±0.25	14.9	6.4
Leu44→Phe/Cys83→Thr/Cys117→Val/Phe132→Trp	0.74±0.19	0.51±0.15	42.6	12.4
Lys12→Val/Cys83→Thr/Cys117→Val	0.93±0.25	0.36±0.12	40.4	19.1

preincubation half-life of 1.0 h; however, with the inclusion of the Cys117→Val mutation, the half-life increases to 9.4 h. Subsequent addition of the Cys83→Thr mutation increases the preincubation half-life to 14.9 h. When this Cys117→Val/Cys83→Thr double mutant is modified further by the addition of either the stabilizing Leu44→Phe/Phe132→Trp double mutant or the stabilizing Lys12→Val point mutant, the half-life increases further to 42.6 and 40.4 h, respectively (Table 4).

Resistance to thiol reactivity, aggregation, and trypsin proteolysis in Tris-buffered saline

The wild-type protein and, to a lesser extent, the Cys117→Val mutant exhibited visible precipitation after 24 and 48 h of incubation at 37 °C in Tris-buffered saline (TBS). The wild-type protein exhibits a general reduction in total soluble protein as a function of incubation time in TBS (Fig. 7a). Furthermore, nonreduced samples indicate the formation of higher-molecular-mass forms, consistent with disulfide-linked multimers, as a function of time. The Cys117→Val mutant (Fig. 7b) yields a slight improvement in the recovery of soluble material as a function of incubation time (see reduced lanes in Fig. 7b), although the presence of higher-mass disulfide-linked forms is evident (see nonreducing lanes in Fig. 7b). The Cys83→Thr/Cys117→Val double mutant improves on the recovery of soluble protein (see reduced lanes in Fig. 7c), and the majority of the soluble protein is present as a monomeric form (see nonreducing lanes in Fig. 7c). This mutant has a single Cys residue at position 16; thus, the higher-mass form visible under nonreducing conditions is consistent with the formation of an intermolecular Cys16-Cys16 disulfide bonded dimer (~36 kDa). The Leu44→Phe/Cys83→Thr/Cys117→Val/Phe132→Trp (Fig. 7d) and Lys12→Val/Cys83→Thr/Cys117→Val (Fig. 7e) mutant proteins show improvements in both recovery of soluble material and fraction of monomeric form in comparison to the Cys83→Thr/Cys117→Val mutant, with the Lys12→Val/Cys83→Thr/Cys117→Val mutant yielding the greatest recovery of soluble monomeric protein after incubation.

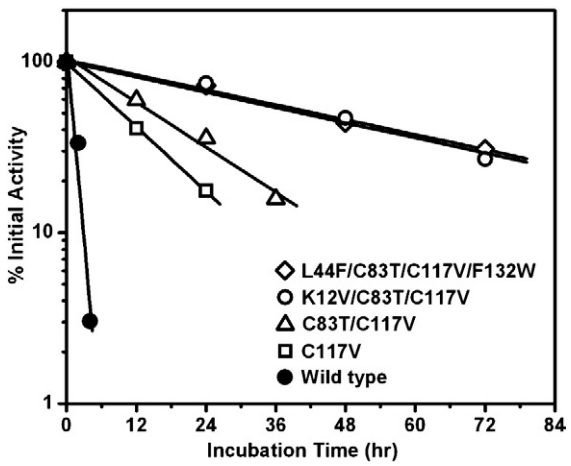

Fig. 6. Inactivation rates of wild-type and mutant forms of FGF-1 in unconditioned DMEM/0.5% NCS at 37 °C. The log of the percent initial mitogenic activity is plotted as a function of incubation time prior to mitogenic assay.

Resistance to trypsin digestion for the wild-type, Cys117→Val, Cys83→Thr/Cys117→Val, Leu44→Phe/Cys83→Thr/Cys117→Val/Phe132→Trp, and Lys12→Val/Cys83→Thr/Cys117→Val mutant proteins is shown in Fig. 8. The associated half-life of the intact protein is given in Table 4. Lys12→Val/Cys83→Thr/Cys117→Val exhibits the greatest resistance to trypsin digestion (with a half-life of 19.1 min under the conditions tested), while the Cys83→Thr/Cys117→Val mutant exhibits the greatest susceptibility to trypsin digestion (with a half-life of 6.4 min).

Discussion

The *in vitro* characterization of the functional half-life of the FGF-1 protein demonstrates an interplay between buried free-cysteine residues and the thermodynamic stability of the protein. The previously reported X-ray structure of wild-type FGF-1[31] shows that the three free cysteines (at positions 16, 83, and 117) are each buried within the protein interior and are 11–19 Å distal to each other (in some crystal forms of FGF-1, Cys117 exhibits an alternative rotamer that is partially solvent accessible). Formation of intermolecular or intramolecular disulfide bonds therefore requires substantial structural rearrangement (as would occur with protein unfolding) and is incompatible with native protein

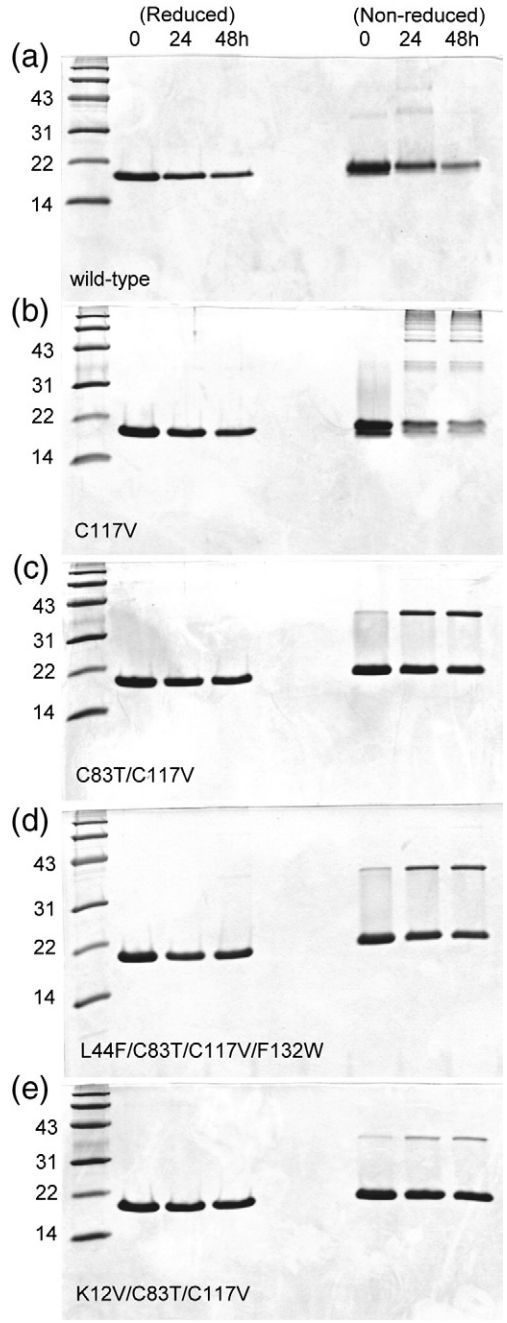

Fig. 7. Coomassie-Brilliant-Blue-stained 16.5% Tricine SDS-PAGE analysis of a time-course incubation of wild-type FGF-1 (a), Cys117→Val (b), Cys83→Thr/Cys117→Val (c), Leu44→Phe/Cys83→Thr/Cys117→Val/Phe132→Trp (d), and Lys12→Val/Cys83→Thr/Cys117→Val (e) in TBS. Samples labeled "reduced" were made in 4% β-mercaptoethanol prior to gel loading.

structure and function. The half-life study of wild-type FGF-1 in unconditioned DMEM/0.5% NCS indicates a functional half-life of 1.0 h. Although the related incubation studies in TBS are not directly comparable on the same timescale (due principally to concentration differences utilized in these assays), the TBS study identifies a physical basis for the observed loss of function. In particular, the incubation study of wild-type FGF-1 in TBS demonstrates loss of soluble monomeric protein as a function of time due to irreversible aggregation; furthermore, the soluble material recovered shows the formation of higher-mass disulfide adducts.

The Cys117→Val mutant eliminates one of three free-cysteine residues in FGF-1 and is associated with an increase in functional half-life in unconditioned DMEM/0.5% NCS from 1.0 to 9.4 h. This point mutant is essentially neutral as regard effects on thermostability; thus, the observed increase in functional half-life is due exclusively to the elimination of a reactive thiol. The incubation of the Cys117→Val mutant in TBS is associated with a marked reduction in visible aggregation, and gel assay shows an increase in the recovery of soluble protein (although disulfide adducts involving Cys16 and Cys83 are clearly present; Fig. 7b). Elimination of a second buried reactive thiol at position Cys83, with the Cys83→Thr/Cys117→Val double mutant, increases the half-life in unconditioned DMEM/0.5% NCS to 14.9 h. The TBS incubation of this mutant shows improved recovery of soluble monomeric protein, and the disulfide adduct is now limited to intermolecular dimer formation involving the remaining thiol at position Cys16. The Cys83→Thr/Cys117→Val mutation is destabilizing compared to the Cys117→Val mutant, and so the observed increase in half-life of this double mutant is due to the elimination of the second buried reactive thiol and not due to an increase in thermostability. The Cys117→Val and Cys83→Thr/Cys117→Val mutants show that the elimination of buried free cysteines within the structure is associated with a substantial and combinatorial increase in *in vitro* half-life. Accessibility of buried thiols requires unfolding of the protein, and disulfide bond formation is an irreversible pathway from the denatured state; such pathways shift the folding equilibrium (via Le

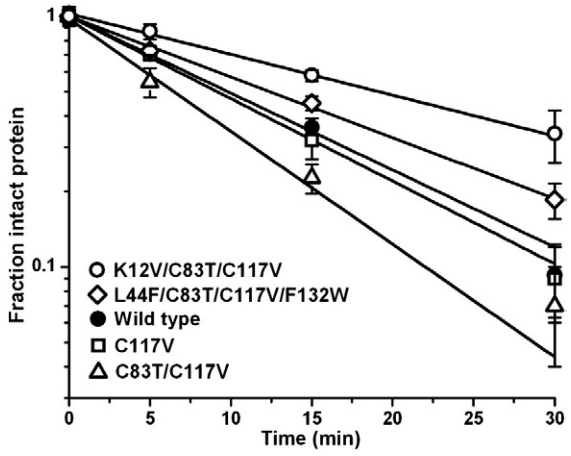

Fig. 8. A time course of the proteolytic digest of wild-type and mutant forms of FGF-1 by trypsin (200:1 molar ratio, respectively) in TBS (pH 7.4) and at 37 °C and quantified by scanning densitometry of Coomassie-Brilliant-Blue-stained Tricine SDS-PAGE.

Chatelier's principle) in the direction of the denatured state.

Comparison of the Cys83→Thr/Cys117→Val, Leu44→Phe/Cys83→Thr/Cys117→Val/Phe132→Trp, and Lys12→Val/Cys83→Thr/Cys117→Val mutant proteins provides an opportunity for evaluating the effects of increasing thermostability under conditions where the number and the type of buried reactive thiols are held constant (in this case, to the single remaining Cys16 residue). In comparison to the Cys83→Thr/Cys117→Val mutant, the Leu44→Phe/Cys83→Thr/Cys117→Val/Phe132→Trp mutant stabilizes the protein by −6.5 kJ/mol, and the Lys12→Val/Cys83→Thr/Cys117→Val mutant stabilizes the protein by −8.3 kJ/mol. Both of these mutants increase the functional half-life in unconditioned DMEM/0.5% NCS in comparison to the Cys83→Thr/Cys117→Val mutant by a factor of 3 (from 14.9 to 42.6 and 40.4 h, respectively). This increase in functional half-life is therefore due exclusively to the increase in thermostability, as no changes to buried thiols have been made. The incubation in TBS shows that this increase in thermostability is associated with a reduction in the formation of disulfide-bonded dimer and a corresponding increase in the soluble monomeric form of the protein (Fig. 7c–e). These results are consistent with the hypothesis that denaturation is necessary for buried free cysteines to become available for disulfide bond formation, and increasing protein stability shifts the folding equilibrium towards the native state, thereby limiting the availability of the buried thiol for reactivity.

The addition of heparin to FGF-1 is known to stabilize the protein and to increase its melting temperature by ~20 °C.[15] The addition of heparin to wild-type FGF-1 increases its potency in the 3T3 fibroblast mitogenic assay by almost 2 orders of magnitude (Table 4). However, the results show that a similar enhancement in mitogenic activity is achieved in the absence of added heparin for those FGF-1 mutant proteins that include the Cys83→Thr/Cys117→Val double mutation (Fig. 5). Furthermore, the Cys117→Val mutation alone provides some enhancement in activity in the absence of added heparin (although not to the extent observed for the double Cys mutants or in comparison to wild-type FGF-1 in the presence of heparin). These results therefore indicate that one of the major effects of the heparin-induced stabilization of FGF-1 is effective curtailment of buried thiol reactivity. We have previously reported that point mutations that substantially stabilize the FGF-1 protein can increase mitogenic potency in the absence of added heparin;[29] the present results suggest that this stability effect on mitogenic activity is due principally to the abolishment of buried thiol reactivity.

Wild-type FGF-1 exhibits relatively poor thermal stability[15,30] and contains three free cysteines within the solvent-excluded core region. The present results demonstrate a functional connection between buried free cysteines and thermostability, such that mutations affecting these properties can modulate the functional half-life. The results show that, in spite of potentially destabilizing effects, if buried thiols are eliminated by mutation, a significant increase in functional half-life is possible. Conversely, if the protein were to realize a substantial gain in thermostability (i.e., due to mutation), the contribution of buried free cysteines to limiting functional half-life would be significantly diminished. Thus, in FGF-1, the combination of relatively low thermal stability and buried free-cysteine residues may represent coevolved properties that cooperate to effectively regulate functional half-life. Similarly, these two properties might be intentionally manipulated in protein design efforts to achieve a targeted functional half-life, a refinement of the "buried free-cysteine" half-life design principle.[32]

Other properties, including susceptibility to proteolytic degradation, may contribute to the observed 3T3 fibroblast mitogenic half-life of mutant FGF-1 proteins. For the set of mutants tested, resistance to trypsin digestion directly correlates with the thermodynamic stability of the protein (Tables 2 and 4). Thus, in addition to limiting the accessibility of buried reactive thiols, increasing thermostability protects the FGF-1 protein from loss of function due to proteolytic degradation. If mutation of buried free cysteines lowers thermodynamic stability, it can increase susceptibility to proteolytic degradation and thereby contribute to a decrease in functional half-life. In the case of Cys83 in FGF-1, a detailed X-ray structure and thermodynamic study shows that the local structural environment is optimized to accept a cysteine at this position, and substitution by other residues results in significant destabilization (with the least disruptive mutation being Cys83→Thr).[28] Thus, combining mutations that eliminate buried free-cysteine residues with mutations that increase thermostability are synergistic in their effect on functional half-life and may be necessary to offset instability associated with cysteine mutations.

Manipulation of thermostability and buried free thiols is of particular interest in the design of "second-generation" protein biopharmaceuticals; however, immunogenic potential as a consequence of mutational change is an important consideration. In the present study, we have asked how substitution of buried free cysteines and stabilization of secondary mutations can be made entirely solvent inaccessible and accommodated with minimal perturbation of the overall wild-type structure, the preferred goal being that the designed mutations eliminate buried thiols and contribute to protein stability but leave the protein's surface features, including solvent structure, indistinguishable from those of wild type. In attempting to achieve this goal, we focused on the design of mutations to fill core-packing defects and thereby to stabilize the protein without introducing changes to the surface structure. In evaluating a total of six core mutations, we were successful with two (Phe132→Trp and a previously described Leu44→Phe mutation) and

"broke even" with one (Phe85→Trp) (Table 2). DSC data indicate that a net gain in van der Waals interactions was realized by the successful subset of aromatic side chain mutations, but that the others (i.e., Phe85→Trp) were accommodated with an actual loss of favorable van der Waals interactions. Thus, the disruption of local van der Waals interactions to accommodate the larger aromatic mutant side chains offset any gain from the additional buried area.

The two successful core mutations were combined to provide ~4 kJ/mol of increased thermostability, which offset an equivalent decrease incurred by the elimination of two of the three buried free cysteines (Cys83→Thr and Cys117→Val); thus, elimination of two buried thiols was accomplished while maintaining overall thermostability and resistance to proteolysis and, most notably, achieving a ~40× increase in functional half-life and eliminating the need for exogenously added heparin to achieve full mitogenic potency. An overlay of the main-chain atoms of this quadruple mutant with those of wild-type FGF-1 from the X-ray structures yields an RMSD of 0.25 Å, essentially identical with a similar overlay involving only those positions within 5.0 Å of the sites of mutation and equivalent to the estimated error of the mutant X-ray data set. Furthermore, a total of 87 conserved solvent molecules distributed over the surface of the wild-type and quadruple-mutant proteins are in essentially identical positions when comparing the two structures (Fig. 9). Thus, the designed mutations within the solvent-excluded region of the protein have been incorporated without perturbing the wild-type surface features, including solvent structure; consequently, the immunogenic potential of this mutant may be correspondingly minimized. This successful design principle—to modulate functional half-life in a potentially immunopermissive manner—is applicable to a broad range of globular proteins that contain a buried free-cysteine residue and core-packing defects.

Materials and Methods

Design, mutagenesis, expression, and purification of recombinant proteins

All studies utilized a synthetic gene for the 140-amino-acid form of human FGF-1[11,31,33,34] containing an additional amino-terminal six His tag, as previously described.[26] Mutations Val31→Ile, Leu44→Trp, Phe85→Trp, Cys117→Ile, and Phe132→Trp were identified as potentially able to fill a subset of existing cavities (cav2, cav4, cav5, cav6, and cav8; Fig. 1) within the core of wild-type FGF-1 by manual model-building methods using wild-type FGF-1 X-ray coordinates (PDB code 1JQZ; molecule A). The QuikChange™ site-directed mutagenesis protocol (Agilent Technologies, Santa Clara, CA) was used to introduce all mutations and was confirmed by nucleic acid sequence analysis (Biomolecular Analysis Synthesis and Sequencing Laboratory, Florida State University). All expressions and purifications followed previously published procedures.[26] Purified protein was exchanged into 50 mM sodium phosphate, 0.1 M NaCl, 10 mM $(NH_4)_2SO_4$, and 2 mM dithiothreitol (DTT; pH 7.5) ("crystallization buffer") for crystallization studies, or into 20 mM *N*-(2-acetamido)iminodiacetic acid (ADA), 0.1 M NaCl, and 2 mM DTT (pH 6.6) ("ADA buffer") for biophysical studies. The yield of most of the mutant proteins was 20–40 mg/L. An extinction coefficient of $E_{280\ nm}$ (0.1%, 1 cm) = 1.26[35,36] was used to determine the protein concentration for wild-type and mutant proteins, with the exception of those mutations involving Trp substitutions. Due to the addition of a novel

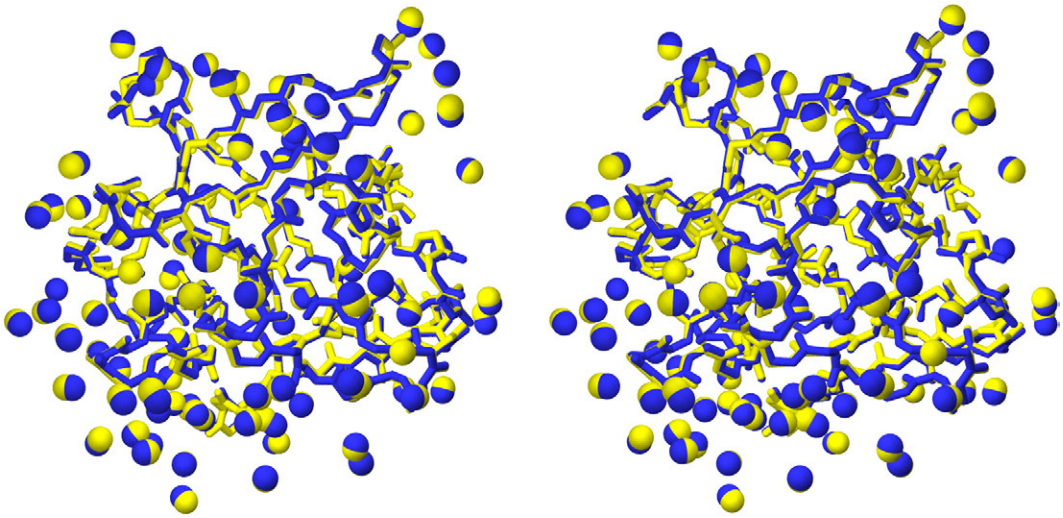

Fig. 9. Relaxed stereo diagram of an overlay of the main-chain atoms of the Leu44→Phe/Cys83→Thr/Cys117→Val/Phe132→Trp mutant (blue) with wild-type FGF-1 (yellow). Also shown (spherical representation) are a set of 87 conserved solvent molecules. The mutant and wild-type structures overlay with an RMSD of 0.25 Å, indicating that the increase in functional half-life provided by the mutations is accommodated with virtually no distortion of the overall protein surface or solvent structure.

Trp fluorophore in these proteins, their extinction coefficients were determined by densitometry analysis of Coomassie-Brilliant-Blue-stained SDS-PAGE of serial dilutions of purified mutant proteins normalized to concentration standards of wild-type FGF-1 (data not shown). The resulting $E_{280\ nm}$ (0.1%, 1 cm) values utilized for all studies were as follows: Leu44→Trp, 1.41; Phe85→Trp, 1.55; Phe132→Trp, 1.58; Leu44→Phe/Phe132→Trp, 1.58; Leu44→Phe/Cys83→Thr/Cys117→Val/Phe132→Trp, 1.58.

Crystallization, X-ray data collection, and refinement of FGF-1 mutant proteins

Purified protein in crystallization buffer was concentrated to 9–13 mg/ml, and crystals were grown using the hanging-drop vapor-diffusion method. Crystals suitable for diffraction grew in 1 week at room temperature with 1.0 ml of reservoir solution containing 2.0–3.5 M sodium formate and 0.1–1.0 M ammonium sulfate in crystallization buffer. Crystals were mounted using Hampton Research nylon-mounted cryoturns and frozen in a stream of gaseous nitrogen at 100 K. Diffraction data were collected using an in-house Rigaku RU-H2R rotating anode X-ray source (Rigaku MSC, The Woodlands, TX) equipped with Osmic Blue confocal mirrors (MarUSA, Evanston, IL) and a Rigaku R-axis IIc image plate detector. Diffraction data were indexed, integrated, and scaled using the DENZO software package.[37,38] His-tagged wild-type FGF-1 (PDB code 1JQZ) was used as search model in molecular replacement for all mutant structures using the CNS software.[39] Model building and visualization utilized the O molecular graphics program.[40] Structure refinement utilized the CNS software, with 5% of the data in the reflection files set aside for R_{free} calculations. Coordinates and structure factors have been deposited in the PDB (coordinate file accession numbers are listed in Table 1). Cavities within the structures were quantified using the Molecular Surfaces Package software[41] and a 1.2-Å-radius probe. The choice of 1.2 Å for the probe radius is slightly larger than the radius of a methyl group (1.1 Å) and identifies cavities that are of significance for possible aliphatic or aromatic point mutations.

Isothermal equilibration denaturation

Isothermal equilibrium denaturation by GuHCl was performed using either fluorescence or circular dichroism (CD) as spectroscopic probe, as previously described.[42] FGF-1 contains a single buried tryptophan residue at position 107, which exhibits atypically greater fluorescence quenching in the native state *versus* the denatured state; this differential fluorescence is used to quantify the unfolding process. Fluorescence data were collected on a Varian Eclipse fluorescence spectrophotometer equipped with a Peltier controlled-temperature regulator at 298 K and using a 1.0-cm pathlength cuvette. Protein samples (5.0 μM) were equilibrated in ADA buffer at 298 K in 0.1 M increments of GuHCl. Triplicate scans were collected and averaged, and buffer traces were collected, averaged, and subtracted from the protein scans. All scans were integrated to quantify the total fluorescence as a function of denaturant concentration.

The Leu44→Trp, Phe85→Trp, Phe132→Trp, Leu44→Phe/Phe132→Trp, and Leu44→Phe/Cys83→Thr/Cys117→Val/Phe132→Trp mutations introduce an additional tryptophan residue in the protein. This additional tryptophan in each case exhibits greater fluorescence quenching in the denatured state; when combined with the endogenous Trp107, atypical fluorescence signal results in an overall fluorescence quenching profile that offers little discrimination between native state and denatured state. A previous study showed that FGF-1 unfolding monitored by CD spectroscopy exhibits an excellent agreement with results obtained by fluorescence spectroscopy and is a useful alternative spectroscopic probe in cases where fluorescence cannot be utilized;[42] therefore, the isothermal equilibrium denaturation profile for the above mutants was characterized using CD spectroscopy. Protein samples (25 μM) were equilibrated in ADA buffer at 298 K in 0.1 M increments of GuHCl. CD data were collected on a Jasco model 810 CD spectrophotometer (Jasco, Inc., Easton, MD) equipped with a Peltier controlled-temperature regulator at 298 K and using a 1-mm pathlength cuvette. For each sample, triplicate scans were collected and averaged, and buffer traces were collected, averaged, and subtracted from sample traces. The unfolding process was monitored by quantifying the change in CD signal at 227 nm with increasing GuHCl.[30] Both fluorescence and CD data were analyzed using the general-purpose nonlinear least-squares fitting program DataFit (Oakdale Engineering, Oakdale, PA) implementing a six-parameter two-state model:[43]

$$F = \frac{F_{0N} + S_N[D] + (F_{0D} + (S_D[D]))e^{-(\Delta G_0 + m[D])/RT}}{1 + e^{-(\Delta G_0 + m[D])/RT}} \quad (1)$$

where [D] is the denaturant concentration; F_{0N} and F_{0D} are the 0 M denaturant intercepts for the native and denatured state baselines, respectively; and S_N and S_D are the slopes of the native and denatured state baselines, respectively. ΔG_0 and m describe the linear function of the unfolding free energy *versus* denaturant concentration. The effect of a given mutation on the stability of the protein ($\Delta\Delta G$) was calculated by taking the difference between the C_m values for wild-type proteins and the C_m values for mutant proteins and multiplying it by the average of the m values, as described by Pace and Scholtz:[44]

$$\Delta\Delta G = (C_{m\,WT} - C_{m\,mutant})(m_{WT} + m_{mutant})/2 \quad (2)$$

where a negative value indicates that the mutation is stabilizing in relationship to the wild-type protein.

Differential scanning calorimetry

All DSC data were collected on a VP-DSC microcalorimeter (GE Healthcare, Piscataway, NJ), as previously described.[30] Briefly, 40 μM protein samples were equilibrated at 298 K in ADA buffer without DTT and in the presence of 0.7 M GuHCl. The inclusion of 0.7 M GuHCl permits reversible two-state thermal denaturation. Protein samples were filtered and degassed for 10 min prior to loading. A scan rate of 15 K/h was used, and the sample was maintained at 30 psi during the calorimetric run. Protein samples were loaded, and all data were collected without interruption of repeated thermal cycles. At least three independent protein scans were collected and averaged, the average of the buffer scans was subtracted, and the resulting scan was normalized to the protein molar concentration. The resulting molar heat capacity profiles were analyzed using the DSCfit software package.[45]

Mitogenic activity and functional half-life in unconditioned medium

Purified protein was equilibrated in 0.14 M NaCl, 5.1 mM KCl, 0.7 mM Na_2HPO_4, and 24.8 mM Tris base (pH 7.4) ("TBS buffer"), and mitogenic activity was evaluated by a cultured fibroblast proliferation assay, as previously described.[29] Briefly, NIH 3T3 fibroblasts were plated in DMEM (Invitrogen, Carlsbad, CA) supplemented with 0.5% (vol/vol) NCS (Sigma-Aldrich Corp., St. Louis, MO) for 48 h at 37 °C with 5% (vol/vol) CO_2. Quiescent serum-starved cells were stimulated with fresh medium supplemented with FGF-1 protein (0–10 μg/ml) and incubated for an additional 48 h. After this incubation period, the cells were counted using a hemacytometer (Hausser Scientific, Horsham, PA). Experiments were performed in quadruplicate, and cell densities were averaged. The protein concentration yielding one-half maximal cell density (EC_{50}) was used for a quantitative comparison of mitogenicity. To evaluate the effect of exogenous heparin on mitogenic potency, we added 10 U/ml heparin sodium salt (Sigma-Aldrich Corp.) to the protein prior to cell stimulation.

For functional half-life studies, the wild-type and mutant FGF-1 proteins were preincubated in unconditioned DMEM/0.5% NCS at 37 °C for various time periods (spanning 0–72 h, depending on the mutant) before being used to stimulate 3T3 fibroblast mitogenic response, as described above. Although the mitogenic assay spans 48 h, the stimulation of FGF receptor in the initial minutes after FGF-1 addition principally dictates the magnitude of the mitogenic response; thus, even comparatively short preincubation periods (i.e., <1 h) can be quantified for loss of functional activity.[11]

Resistance to thiol reactivity, aggregation, and trypsin proteolysis in TBS

Wild-type and mutant proteins at a concentration of 0.25 mg/ml were incubated at 37 °C in TBS buffer and evaluated for disulfide bond formation and aggregation. Samples taken at time points of 0, 24, and 48 h were centrifuged at 10,000*g* for 5 min, and the soluble fraction was mixed with SDS sample buffer (both with and without 4% β-mercaptoethanol), resolved on 16.5% *N*-[2-hydroxy-1,1-bis(hydroxymethyl)ethyl]glycine (Tricine) SDS-PAGE, and visualized with Coomassie Brilliant Blue staining. Stained gels were scanned, and the amounts of soluble monomeric protein and disulfide-linked multimers were quantified using UN-SCAN-IT densitometry software (Silk Scientific, Orem, UT).

Wild-type and mutant proteins were incubated with trypsin (Sigma-Aldrich Corp.) (200:1 molar ratio, respectively) in TBS buffer at 37 °C to evaluate resistance to proteolysis. Time points were taken at 0, 5, 15, and 30 min and resolved on 16.5% Tricine SDS-PAGE visualized with Coomassie Brilliant Blue staining. Stained gels were scanned, and the amount of intact protein was quantified using UN-SCAN-IT densitometry software (Silk Scientific).

Accession numbers

Coordinates and structure factors have been deposited in the PDB with accession numbers 3FJC, 3FJ9, 3FJA, 3FJB, 3FJ8, 3FJD, and 3FGM.

Acknowledgements

We thank Dr. T. Somasundaram (X-ray Crystallography Facility) and Dr. Claudius Mundoma (Physical Biochemistry Facility, Kasha Laboratory, Institute of Molecular Biophysics) for valuable suggestions and technical assistance. We also thank Ms. Pushparani Dhanarajan (Molecular Cloning Facility, Department of Biological Science) for helpful comments. We acknowledge the instrumentation facilities of the Biomedical Proteomics Laboratory, College of Medicine. This work was supported by grant 0655133B from the American Heart Association. All X-ray structures have been deposited in the PDB.

References

1. Crommelin, D. J. A., Storm, G., Verrijk, R., de Leede, L., Jiskoot, W. & Hennink, W. E. (2003). Shifting paradigms: biopharmaceuticals *versus* low molecular weight drugs. *Int. J. Pharm.* **266**, 3–16.
2. BIO. (2007). Biotechnology Industry Organization. www.bio.org.
3. Krishnamurthy, R. & Manning, M. C. (2002). The stability factor: importance in formulation development. *Curr. Pharm. Biotechnol.* **3**, 361–371.
4. Hermeling, S., Crommelin, D. J. A., Schellekens, H. & Jiskoot, W. (2004). Structure–immunogenicity relationships of therapeutic proteins. *Pharm. Res.* **21**, 897–903.
5. Frokjaer, S. & Otzen, D. E. (2005). Protein drug stability: a formulation challenge. *Nat. Rev.* **4**, 298–306.
6. Hochuli, E. (1997). Interferon immunogenicity: technical evaluation of interferon-alpha 2a. *J. Interferon Cytokine Res.* **17**, S15–S21.
7. Moore, W. V. & Leppert, P. (1980). Role of aggregated human growth hormone (hGH) in development of antibodies to hGH. *J. Clin. Endocrinol. Metab.* **51**, 691–697.
8. Purohit, V. S., Middaugh, C. R. & Balasubramanian, S. V. (2006). Influence of aggregation on immunogenicity of recombinant human Factor VIII in hemophilia A mice. *J. Pharm. Sci.* **95**, 358–371.
9. Perry, L. J. & Wetzel, R. (1987). The role of cysteine oxidation in the thermal inactivation of T4 lysozyme. *Protein Eng.* **1**, 101–105.
10. McRee, D. E., Redford, S. M., Getzoff, E. D., Lepock, J. R., Hallewell, R. A. & Tainer, J. A. (1990). Changes in crystallographic structure and thermostability of a Cu, Zn superoxide dismutase mutant resulting from the removal of a buried cysteine. *J. Biol. Chem.* **265**, 14234–14241.
11. Ortega, S., Schaeffer, M. -T., Soderman, D., DiSalvo, J., Linemeyer, D. L., Gimenez-Gallego, G. & Thomas, K. A. (1991). Conversion of cysteine to serine residues alters the activity, stability, and heparin dependence of acidic fibroblast growth factor. *J. Biol. Chem.* **266**, 5842–5846.
12. Faletto, M. B., Linko, P. & Goldstein, J. A. (1992). A single amino acid mutation (Ser180-Cys) determines the polymorphism in cytochrome P450g (P4502C13) by altering protein stability. *J. Biol. Chem.* **267**, 2032–2037.
13. Fremaux, I., Mazeres, S., Brisson-Lougarre, A., Arnaud, M., Ladurantie, C. & Fournier, D. (2002).

Improvement of *Drosophila* acetylcholinesterase stability by elimination of a free cysteine. *BMC Biochem.* **3**, 21.
14. Petersen, M. T. N., Jonson, P. H. & Petersen, S. B. (1999). Amino acid neighbours and detailed conformational analysis of cysteines in proteins. *Protein Eng.* **12**, 535–548.
15. Copeland, R. A., Ji, H., Halfpenny, A. J., Williams, R. W., Thompson, K. C., Herber, W. K. *et al.* (1991). The structure of human acidic fibroblast growth factor and its interaction with heparin. *Arch. Biochem. Biophys.* **289**, 53–61.
16. Engleka, K. A. & Maciag, T. (1992). Inactivation of human fibroblast growth factor-1 (FGF-1) activity by interaction with copper ions involves FGF-1 dimer formation induced by copper-catalyzed oxidation. *J. Biol. Chem.* **267**, 11307–11315.
17. Estape, D., van den Heuvel, J. & Rinas, U. (1998). Susceptibility towards intramolecular disulphide-bond formation affects conformational stability and folding of human basic fibroblast growth factor. *Biochem. J.* **335**, 343–349.
18. Gospodarowicz, D. & Cheng, J. (1986). Heparin protects basic and acidic FGF from inactivation. *J. Cell. Physiol.* **128**, 475–484.
19. Harris, J. M. & Chess, R. B. (2003). Effect of PEGylation on pharmaceuticals. *Nat. Rev. Drug Discov.* **2**, 214–221.
20. Haag, R. & Kratz, F. (2006). Polymer therapeutics: concepts and applications. *Angew. Chem. Int. Ed.* **45**, 1198–1215.
21. Chapman, A. P. (2002). PEGylated antibodies and antibody fragments for improved therapy: a review. *Adv. Drug Deliv. Revi.* **54**, 531–545.
22. Basu, A., Yang, K., Wang, M., Liu, S., Chintala, R., Palm, T. *et al.* (2006). Structure–function engineering of interferon-β-1b for improving stability, solubility, potency, immunogenicity, and pharmacokinetic properties by site-selective mono-PEGylation. *Bioconjug. Chem.* 17.
23. Monfardini, C., Schiavon, O., Caliceti, P., Morpurgo, M., Harris, J. M. & Veronese, F. M. (1995). A branched monomethoxypoly(ethylene glycol) for protein modification. *Bioconjug. Chem.* **6**, 62–69.
24. Kurtzman, A. L., Govindarajan, S., Vahle, K., Jones, J. T., Heinrichs, V. & Patten, P. A. (2001). Advances in directed protein evolution by recursive genetic recombination: applications to therapeutic proteins. *Curr. Opin. Biotechnol.* **12**, 361–370.
25. Murzin, A. G., Lesk, A. M. & Chothia, C. (1992). β-Trefoil fold. Patterns of structure and sequence in the kunitz inhibitors interleukins-1β and 1α and fibroblast growth factors. *J. Mol. Biol.* **223**, 531–543.
26. Brych, S. R., Blaber, S. I., Logan, T. M. & Blaber, M. (2001). Structure and stability effects of mutations designed to increase the primary sequence symmetry within the core region of a β-trefoil. *Protein Sci.* **10**, 2587–2599.
27. Brych, S. R., Kim, J., Logan, T. M. & Blaber, M. (2003). Accommodation of a highly symmetric core within a symmetric protein superfold. *Protein Sci.* **12**, 2704–2718.
28. Lee, J. & Blaber, M. (2009). Structural basis of conserved cysteine in the fibroblast growth factor family: evidence for a vestigial half-cystine. *J. Mol. Biol.* in press. doi:10.1016/j.jmb.2009.08.007.
29. Dubey, V. K., Lee, J., Somasundaram, T., Blaber, S. & Blaber, M. (2007). Spackling the crack: stabilizing human fibroblast growth factor-1 by targeting the N and C terminus beta-strand interactions. *J. Mol. Biol.* **371**, 256–268.
30. Blaber, S. I., Culajay, J. F., Khurana, A. & Blaber, M. (1999). Reversible thermal denaturation of human FGF-1 induced by low concentrations of guanidine hydrochloride. *Biophys. J.* **77**, 470–477.
31. Blaber, M., DiSalvo, J. & Thomas, K. A. (1996). X-ray crystal structure of human acidic fibroblast growth factor. *Biochemistry*, **35**, 2086–2094.
32. Culajay, J. F., Blaber, S. I., Khurana, A. & Blaber, M. (2000). Thermodynamic characterization of mutants of human fibroblast growth factor 1 with an increased physiological half-life. *Biochemistry*, **39**, 7153–7158.
33. Gimenez-Gallego, G., Conn, G., Hatcher, V. B. & Thomas, K. A. (1986). The complete amino acid sequence of human brain-derived acidic fibroblast growth factor. *Biochem. Biophys. Res. Commun.* **128**, 611–617.
34. Linemeyer, D. L., Menke, J. G., Kelly, L. J., Disalvo, J., Soderman, D., Schaeffer, M. -T. *et al.* (1990). Disulfide bonds are neither required, present, nor compatible with full activity of human recombinant acidic fibroblast growth factor. *Growth Factors*, **3**, 287–298.
35. Zazo, M., Lozano, R. M., Ortega, S., Varela, J., Diaz-Orejas, R., Ramirez, J. M. & Gimenez-Gallego, G. (1992). High-level synthesis in *Escherichia coli* of a shortened and full-length human acidic fibroblast growth factor and purification in a form stable in aqueous solutions. *Gene*, **113**, 231–238.
36. Tsai, P. K., Volkin, D. B., Dabora, J. M., Thompson, K. C., Bruner, M. W., Gress, J. O. *et al.* (1993). Formulation design of acidic fibroblast growth factor. *Pharm. Res.* **10**, 649–659.
37. Otwinowski, Z. (1993). In (Sawyer, L., Isaacs, N. & Bailey, S., eds), pp. 55–62, SERC Daresbury Laboratory, Warrington, UK.
38. Otwinowski, Z. & Minor, W. (1997). Processing of X-ray diffraction data collected in oscillation mode. *Methods Enzymol.* **276**, 307–326.
39. Brunger, A. T., Adams, P. D., Clore, G. M., DeLano, W. L., Gros, P., Grosse-Kunstleve, R. W. *et al.* (1998). Crystallography and NMR system (CNS): a new software system for macromolecular structure determination. *Acta Crystallogr. Sect. D*, **54**, 905–921.
40. Johnson, D. E., Lu, J., Chen, H., Werner, S. & Williams, L. T. (1991). The human fibroblast growth factor receptor genes: a common structural arrangement underlies the mechanisms for generating receptor forms that differ in their third immunoglobulin domain. *Mol. Cell. Biol.* **11**, 4627–4634.
41. Connolly, M. L. (1993). The molecular surface package. *J. Mol. Graphics*, **11**, 139–141.
42. Kim, J., Brych, S. R., Lee, J., Logan, T. M. & Blaber, M. (2003). Identification of a key structural element for protein folding within β-hairpin turns. *J. Mol. Biol.* **328**, 951–961.
43. Eftink, M. R. (1994). The use of fluorescence methods to monitor unfolding transitions in proteins. *Biophys. J.* **66**, 482–501.
44. Pace, C. N. & Scholtz, J. M. (1997). Measuring the conformational stability of a protein. In (Creighton, T. E., ed.), pp. 299–321, Oxford University Press, Oxford.
45. Grek, S. B., Davis, J. K. & Blaber, M. (2001). An efficient, flexible-model program for the analysis of differential scanning calorimetry protein denaturation data. *Protein Pept. Lett.* **8**, 429–436.